Research article

Chengkun Yang, Hao Zhang*, Bo Liu*, Haifeng Liu, Chao Wang and Shiwei Lin

Electrically tuned whispering gallery modes microresonator based on microstructured optical fibers infiltrated with dual-frequency liquid crystals

Abstract: An electrically tunable whispering gallery mode (WGM) microresonator based on an HF-etched microstructured optical fiber (MOF) infiltrated with dual-frequency liquid crystals (DFLCs) is proposed and experimentally demonstrated for the investigation of the crossover frequency and Freedericksz transition of DFLCs. Experimental results indicate that for applied electric field with operation frequency below the crossover frequency, WGM resonance wavelength decreases with the increment of applied electric field strength. On the contrary, for applied electric field with operation frequency beyond the crossover frequency, WGM resonance dips show red shift as the applied electric field intensity increases. The proposed electrically tunable microcavity integrated with DFLCs is anticipated to find potential applications in optical filtering, all-optical switching, and electrically manipulated bi-directional micro-optics devices.

Keywords: liquid crystal; microstructured optical fiber (MOF); optical microresonator; whispering gallery mode (WGM).

1 Introduction

Whispering gallery mode (WGM) microresonators are axially symmetric structures that trap light inside based on total internal reflection effect at the interface between the microresonator and the surrounding medium. A wide range of optical microresonators, such as microsphere [1], microbottles [2], micro-disks [3], micro-ring [4], and cylindrical microcavities [5], have attracted growing worldwide research interest. Due to their high optical quality, enhanced optical field, and small mode volume, optical microresonators have found various potential applications in optical filters [6, 7], low-threshold microlasers [8], as well as high sensitivity biological and chemical sensors [9, 10]. It should be noted that WGM properties are generally determined by the relative index of refraction of the microresonator and its surrounding medium. With regard to practical applications, the spectral tunability of a silica microresonator is imperative for photonic devices. A good variety of tunable WGM devices have been developed by controlling the ambient temperature [11], refraction index [12], as well as geometry of the microresonator [13]. There are also some reports on the investigation of microresonators based on water [14], glycerol [15], and magnetic fluids [16–18]. However, the tuning of modes in these microresonators is not easy in the sense that their resonance mode frequencies cannot be changed easily or exhibit rather small shift. Recent studies on optical microcavities based on liquid crystals (LCs) [19, 20] provide promising WGM tuning schemes by changing environmental temperature or applied electric field intensity to achieve large wavelength shifts. Due to the ease of deformation of PDMS coating under external force, the shape of the microresonator would change when strong electric field is applied, which may have a great impact on WGM characteristics. In a paper [21], we proposed that in a microresonator filled with nematic LC, the shape of the microresonator will not change at high applied electric field. All of these tuning methods were only able to achieve resonance wavelength shift toward a shorter wavelength or longer wavelength region.

In this paper, we propose and experimentally demonstrate an electrically tuned microstructured optical fiber (MOF) microresonator integrated with dual-frequency liquid crystals (DFLCs). A segment of grapefruit MOF serves as a cylindrical microresonator where the WGMs are excited by evanescent coupling of light propagating through a thin fiber taper placed perpendicularly and in

Corresponding authors: Hao Zhang and Bo Liu, Tianjin Key Laboratory of Optoelectronic Sensor and Sensing Network Technology, Institute of Modern Optics, Nankai University, Tianjin 300350, China, e-mail: haozhang@nankai.edu.cn (H. Zhang); liubo@nankai.edu.cn (B. Liu)
Chengkun Yang, Haifeng Liu and Shiwei Lin: Tianjin Key Laboratory of Optoelectronic Sensor and Sensing Network Technology, Institute of Modern Optics, Nankai University, Tianjin 300350, China
Chao Wang: School of Engineering and Digital Arts, University of Kent, Canterbury CT2 7NT, United Kingdom

direct contact with the MOF. Our work aims to propose an optical microresonator to achieve WGM resonance shift toward shorter and longer wavelength regions in the meantime based on electric field tuning approach.

2 Experimental setup

The experimental setup of testing the proposed MOF-based WGM microresonator infiltrated with DFLCs is shown in Figure 1. A continuous wave light from 1530 nm to 1560 nm with wavelength step of 0.5 pm is generated by a tunable laser (TL, KEYSIGHT, 8164B, USA). The polarization of light was adjusted by a polarization controller (PC, KEYSIGHT, N7786B, USA). The output spectra were measured with an optical power meter (OPM, KEYSIGHT, N7744A, USA). Meanwhile, the spectral information is transferred to a laptop for data processing.

    The fiber used in our experiments is grapefruit MOF with six rings of air holes of 15 μm around its asymmetric solid core. LCs are infiltrated into the MOF air holes in the presence of capillary forces by dipping one end of the fiber into DFLCs. The whole experimental process is carried out at room-temperature and pressure conditions. Two DFLC samples are employed in this study: DFLC-1 (HEF951800-100, HCCH, China) with an optical birefringence $\Delta n = 0.218$ at 25°C and phase transition temperature of 104.3°C and DFLC-2 (DP002-026, HCCH, China) with an optical birefringence $\Delta n = 0.263$ at 25°C and phase transition temperature of 117°C. As WGMs are
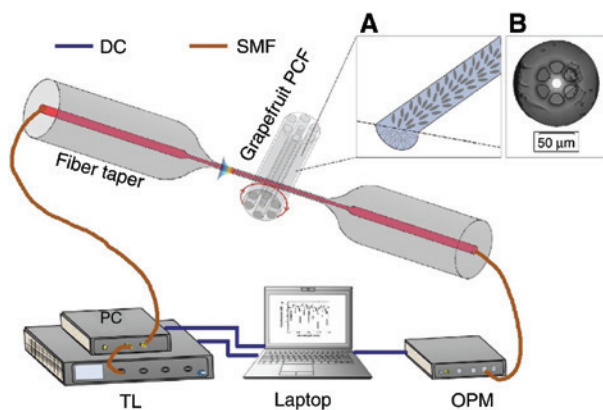

Figure 2: Polarized micrographs of silica capillaries (inner diameter, 30 μm) infiltrated with DFLCs.
Capillaries angled at 0° (A) and 45° (B) with respect to the polarizer axis.

normally traveling close to the outer periphery of the circular optical microcavity in order to enhance the sensitivity of WGM properties to the refractive index variation of the LCs kept inside the air holes, the silica background of the grapefruit MOF is partially etched with hydrofluoric acid at a concentration of 40% by weight. The diameter of the HF-etched MOFs infiltrated with LCs is about 63.5 μm, and the gap between the holes and the outer surface is about 1.75 μm. In this case, the variation of cross-sectional refractive index distribution caused by the orientations of the LC molecules would cause the change of WGMs traveling along the outer periphery of the MOF microresonator. In general, the orientation of the LC molecules is determined by the surface anchoring energy of the LCs and the applied electric field intensity. Many optical [22, 23] and nuclear magnetic resonance [24, 25] studies reveal that the orientation of the LC molecules in cylindrical cavities with radius diameter between 0.5 and 200 μm would exhibit the escaped radial structure [26]. In the escaped radial structure, LC molecules will be orientated with an angle of less than 90° with respect to the inner surface of the air holes and turns to be orientated parallel to the inclusion axis around the central area, as shown in Figure 1A. Figure 2 shows the images of the capillaries infiltrated with DFLCs captured by using a polarized microscope, which indicate that the LC molecules are in an escaped radial structure [25].

Figure 1: The experimental setup for performance testing of the proposed MOF-based microresonator integrated with LCs.
DC, Data cable; grapefruit PCF, grapefruit photonic crystal fiber; PC, polarization controller; OPM, optical power meter; SMF, single-mode fiber; TL, tunable laser. Insets (A) and (B) show the schematic orientation of LC molecules in the grapefruit MOF and the cross-sectional microscopic grapefruit MOF, respectively.
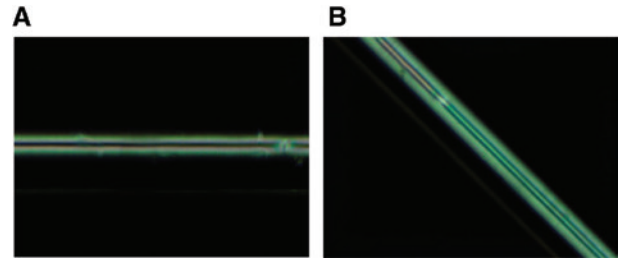
3 Theoretical analysis

In Figure 3, WGMs in optical microcavities are characterized by two types of polarization components, namely, TE mode and TM mode, where the electric field oscillates perpendicular and parallel to the cross-section of the microresonator, respectively. By adjusting the polarization state of the incident laser light, WGM resonances could
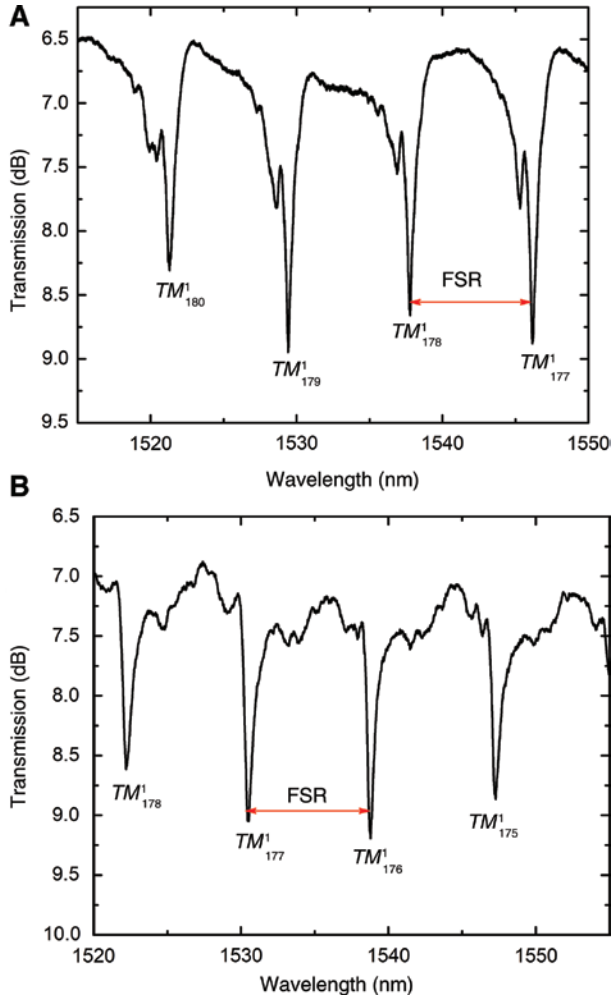
Figure 3: Experimental WGM transmission spectra for the MOF microresonators respectively infiltrated with (A) DFLC-1 and (B) DFLC-2 in the absence of electric field.

be clearly acquired in the transmission spectrum in the absence of electric field, as the microresonator is coupled with the tapered fiber waveguide, as shown in Figure 3.

By adjusting the polarization state of the incident light, we have only acquired the WGM transmission spectra for TM modes, as shown in Figure 3. To theoretically analyze the WGM transmission characteristics, the resonant wavelength is satisfied with the asymptotic formula in cylindrical microresonators [27, 28]:

$$\text{n}\frac{2\pi r n_2}{\lambda} = m + 2^{-1/3} a_l m^{1/3} - \frac{P}{(n^2-1)^{1/2}} + \frac{3}{10} 2^{-2/3} a_l^2 m^{-1/3}$$
$$- \frac{2^{-1/3} P(n^2 - 2P^2/3)}{(n^2-1)^{3/2}} a_l m^{-2/3} + \text{O}(m^{-1}), \quad (1)$$

where r is the inner radius of the mircroresonator; $m \gg 1$ is the angular mode order; $l=1, 2, 3\ldots$ is the radial mode number of WGMs; n_2 is the index of pure silica; n_1 is the

effective index of the medium inside the microresonator; $n = n_1/n_2$; $P = n_1/n_2 = m$ for the TM mode while $P = n_2/n_1 = 1/m$ for the TE mode; a_l is l – the zeroth order of Airy function.

According to the experimental spectral data in Figure 3, mode numbers of l, with m relating to specific polarization state, are fitted by using Eq. (1), showing that the experimentally observed WGM transmission spectrum results from a TM wave and the mode number (l, m) should be (1, 177–180) and (1, 175–178) for microresonators infiltrated with DFLC-1 and DFLC-2, respectively. As shown in Figure 3, resonance dips correspond to the fundamental WGMs and no higher radial order ($l \geq 2$) modes are excited due to the fact that the grapefruit MOF wall thickness is thin enough to suppress higher order WGMs. The free spectral ranges (FSR) between adjacent WGM peaks increase with the increment of WGM resonance wavelength. The experimental measured FSRs for microresonator filled with DFLC-1 between these four WGM resonance peaks are 8.1365 nm, 8.3525 nm, and 8.387 nm, respectively, which are in agreement with the calculated results of 8.1752 nm, 8.264 nm, and 8.3545 nm. And for the microresonator filled with DFLC-2, the experimental measured FSRs for these four WGM resonance peaks are 8.2945 nm, 8.2955 nm, and 8.483 nm, respectively, which agree well with the calculated results of 8.2701 nm, 8.361 nm, and 8.4535 nm.

To quantitatively characterize the resonance spectra, Lorentz fitting is performed on the WGM transmission spectra for the TM_{177}^1 mode for the microresonators infiltrated with DFLC-1 and DFLC-2, as shown in Figure 4A and B, respectively. The quality factor of the proposed microresontator could be calculated by using $Q = \lambda/\Delta\lambda$, where λ is resonance wavelength and $\Delta\lambda$ refers to full width at half-maximum (FWHM) of the resonance peak. As shown in Figure 4, when no electric field is applied, the Q-factors for the grapefruit MOF microresonators infiltrated with DFLC-1 and DFLC-2 are 2.707×10^3 and 2.598×10^3, respectively. These Q-factors are in the same magnitude of typical LC-infiltrated cylindrical micro-resonators [21, 29], and the relatively low Q-factors mainly result from strong scattering of LC molecules.

Different from conventional LCs with single operation frequency, DFLCs show a unique feature in that their dielectric anisotropy ($\Delta\varepsilon$) turns from positive value at low frequencies to negative value as the operation frequency passes by the crossover frequency (f_c) [30, 31], as shown in Figure 5. The frequency-dependent reversible dielectric anisotropy makes it possible to align the DFLC molecules along or perpendicular to the electric field direction by adjusting the frequency of the driving electric signals. At low frequencies, $f < f_c$ ($\Delta\varepsilon > 0$), the rotation of the molecules
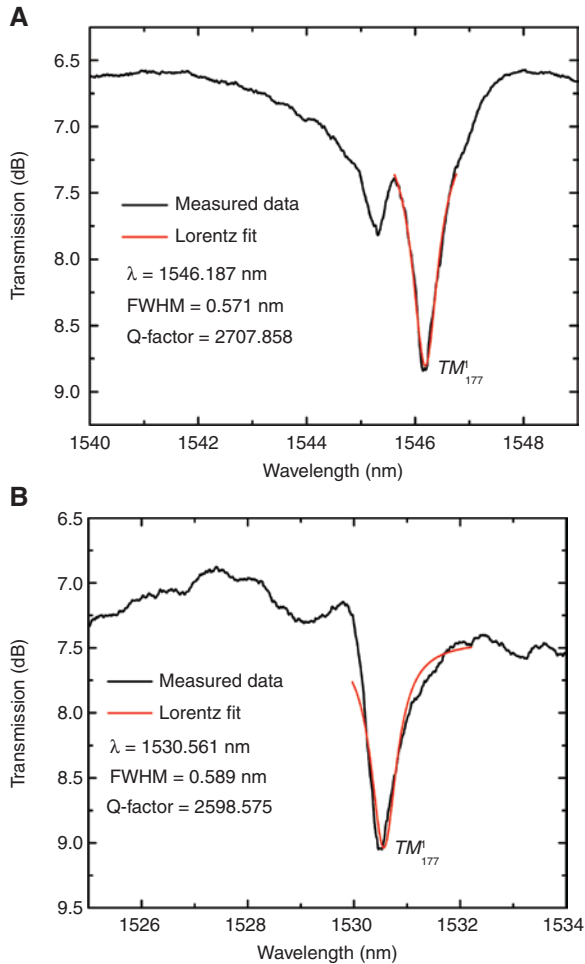
A

B

Figure 4: Lorentzian fitting of the WGM transmission spectra for TM^1_{177} modes with estimated Q-factors for the two grapefruit MOF microresonators, respectively, infiltrated with (A) DFLC-1 and (B) DFLC-2 in the absence of electric field at room temperature.
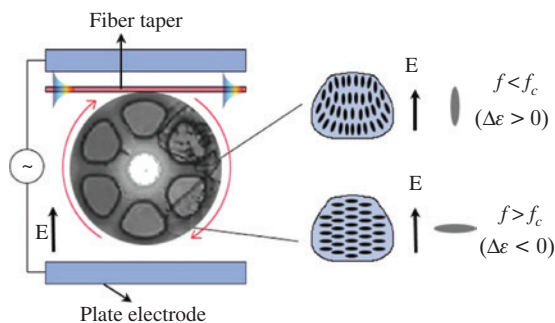

Figure 5: Cross-section of the grapefruit-MOF-based microresonator sandwiched between two electrodes and effect of an electric field on a DFLC at different frequencies.

around their short axis is unhindered and the molecules align parallel to the electric field. However, at higher frequencies, $f > f_c$ ($\Delta\varepsilon < 0$), only the transverse components

of the molecular dipole moments are dominant, and consequently, the molecules would orient perpendicularly to the applied electric field. At crossover frequency, $f = f_c$ ($\Delta\varepsilon = 0$), dielectric anisotropy of DFLCs disappears. These intriguing features indicate that it is possible to achieve WGM resonance wavelength shift toward longer as well as shorter wavelength region in the meantime based on the frequency-dependent anisotropic transition mechanism.

To analyze the electric tuning characteristics of the proposed MOF-based microcavity infiltrated with DFLCs, the part of the fiber containing the DFLC is sandwiched between two electrodes with applied AC electric field. With no electric field applied, the distribution of LC molecules in microresonator is an escaped radial structure, and with the strengthening of the applied electric field at low frequencies, $f < f_c$, the molecules located close to the interior surface of the microcavity tend to gradually align in the electric field direction. When the applied electric field operates at higher frequencies, $f > f_c$, the molecules located close to the interior surface of the microcavity tend to gradually align perpendicularly to the electric field direction. The realignment of LCs molecules would change the effective refractive index of microresonator, leading to the WGM resonance dips shifting to shorter or longer wavelength region.

4 Experimental results and discussion

For the grapefruit-MOF-based microresonator filled with DFLC-1, the WGM resonance dips move toward shorter wavelength region as the applied electric field frequency increases from 0.5 kHz to 10 kHz. At 30 kHz and 40 kHz, the resonance wavelength shifts toward longer wavelength region with the strengthening of the applied electric field; at 20 kHz, the WGM resonance wavelengths exhibit irregular fluctuations with the increment of the applied electric field intensity, as shown in Figure 6. At 0.5 kHz and 40 KHz, the WGM resonance dips shift by 2.628 nm and 0.64 nm, respectively. It could be found that below 20 kHz, WGM resonance dips shift toward shorter wavelength region as the applied electric field intensity gradually increases, while above this particular frequency, WGM resonance dips show wavelength shift in opposite direction. From Figure 6C, it could be seen that the crossover frequency of DFLC-1 is about 20 kHz.

We have also investigated the frequency-dependent resonance wavelength shift behavior for the grapefruit-MOF-based microresonator filled with DFLC-2, as shown in
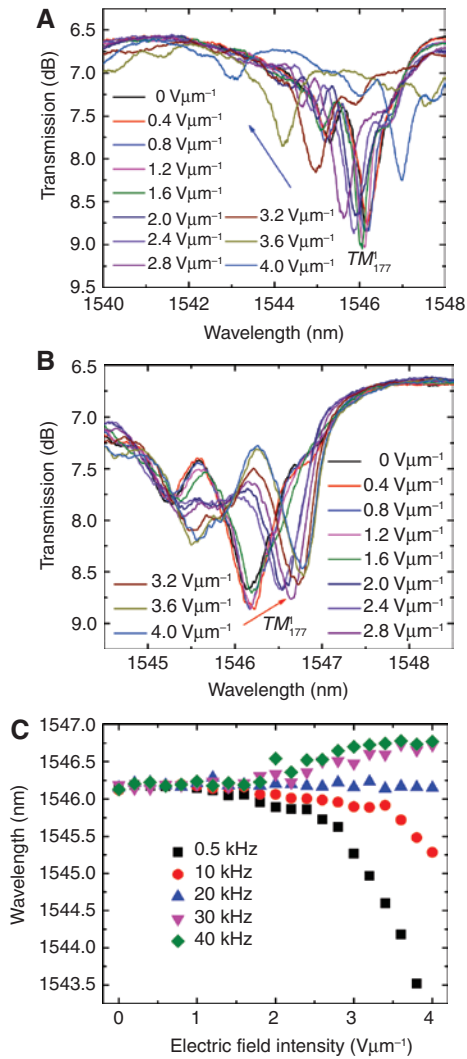
Figure 6: Transmission spectra of the grapefruit-MOF-based microresonator filled with DFLC-1 under the applied electric field at (A) 0.5 kHz and (B) 40 kHz, respectively. Arrows in these figures indicate the spectral shift direction with the increment of the applied electric field intensity. (C) WGM resonance wavelength shift as functions of applied electric field for different AC signal frequencies.

Figure 7: Transmission spectra of the grapefruit-MOF-based microresonator filled with DFLC-2 under the applied electric field at (A) 10 kHz and (B) 50 kHz, respectively. Arrows in these figures indicate the spectral shift direction with the increment of the applied electric field intensity. (C) WGM resonance wavelength shift as functions of applied electric field for different AC signal frequencies.

Figure 7. It is apparent that at 10 kHz and 20 kHz, the WGM resonance dips shift toward shorter wavelength region as the applied electric field intensity gradually increases, while at 30 kHz, 40 kHz, and 50 kHz, the resonance dips shift toward longer wavelength region. At 10 kHz and 50 kHz, the WGM resonance dips shift by 1.7615 nm and 0.8225 nm, respectively. From Figure 7, it could be seen that below 20 kHz, WGM resonance dips shift toward shorter wavelength region as the applied electric field intensity gradually increases, while above 30 kHz, WGM resonance dips show opposite wavelength shift behavior. Therefore, the crossover frequency of DFLC-2 should be located between 20 kHz and 30 kHz.
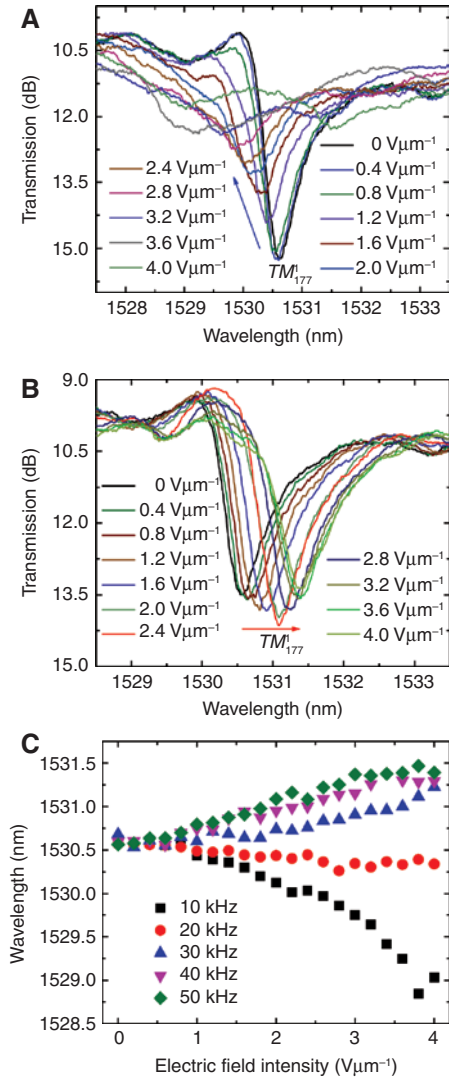
Crossover frequency is one of the most important indicators to evaluate the performances of DFLC. DFLC is an LC mixture whose $\varepsilon_{||}$ (or ε_e) is highly dependent on the operation frequency normally ranging from kHz to MHz while $\varepsilon_{\perp}$ (or ε_o) is frequency independent within the above specific frequency range. Therefore, the dielectric anisotropy of DFLCs is positive at low frequencies while turns to be negative at high frequencies. The frequency where dielectric anisotropy changes its sign ($\Delta\varepsilon = 0$) is called crossover frequency (f_c). The dielectric anisotropies of DFLC-1 and DFLC-2 at different frequencies are given in Table 1. The crossover frequency of DFLC-1 is between 10 kHz and 20 kHz at a temperature of 20°C, and the crossover

Frequency (f)	0.5 kHz	10 kHz	20 kHz	30 kHz	40 kHz	50 kHz
DFLC-1 (Δε)	2.06	0.93	−0.28	−0.02		
DFLC-2 (Δε)		2.3	−0.1	−1.6	−2.4	−2.8

frequency of DFLC-2 is about 20 kHz at a temperature of 20°C. The frequency of the applied electric field has great influence on the orientation of LC molecules. When $f < f_c$, the molecular orientation aligns parallel to the electric field direction and the WGM resonance dips shift toward shorter wavelength region as the applied electric field intensity gradually increases. When $f > f_c$, the molecular orientation tends to be perpendicular to the electric field direction and the WGM resonances dips move towards longer wavelength region with the strengthening of the applied electric field. From Figure 6C, it could be seen that for the MOF microresonator filled with DFLC-1, when the operation frequency is less than 20 kHz, WGM resonance dips shift toward shorter wavelength region, while when the frequency is larger than 20 kHz, WGM resonance move toward longer wavelength region; at 20 kHz, the WGM resonance dips almost do not exhibit any wavelength shift. Therefore, the crossover frequency of DFLC-1 is about 20 kHz, which is larger than the value in Table 1. From Figure 7C, it could be seen that for DFLC-2, when the frequency is less than 20 kHz, WGM resonance dips shift toward shorter wavelength region, while when the frequency is larger than 30 kHz, WGM resonance dips shift in the opposite direction. In this case, the crossover frequency of DFLC-2 should be located between 20 kHz and 30 kHz, which is also larger than the value in Table 1. The deviation of the experimentally acquired crossover frequencies of the DFLCs from the values in Table 1 could be attributed to the great impact of temperature on electrical and optical properties of DFLCs. The value of Δε decreases while f_c increases with the increment of temperature, making the crossover frequency strongly temperature-dependent. As temperature increases, the crossover frequency would increase exponentially [31]. As our experiment is conducted at 26°C, the experimentally acquired crossover frequencies turn to be larger than those in Table 1.

Besides the frequency-dependent birefringence effect, Freedericksz transition [32] is also a fundamental phenomenon taking place in many LC-based devices, which is affected by the surface anchoring, elastic torque, electric field induced torque, as well as viscous torque of the LC devices and is known for the feature that LC molecules could be re-orientated in case the applied electric field

intensity is beyond the Freedericksz transition threshold. As shown in Figures 6C and 7C, when the applied electric field intensity is not high enough, WGM resonance wavelengths exhibit irregular fluctuations. However, when the applied electric field intensity is beyond the Freedericksz transition threshold, WGM resonance wavelengths would exhibit regular shift with the increment of the applied electric field intensity. From Figures 6C and 7C, it could be found that the Freedericksz transition thresholds for DFLC-1 and DFLC-2 are about 1.8 V μm^{-1} and 1.0 V μm^{-1}, respectively.

To investigate the frequency-dependent WGM tuning characteristics of the grapefruit-MOF-based microresonators infiltrated with different LCs, we have investigated WGM resonance wavelengths as functions of applied electric signal frequency for different electric field intensities, as shown in Figure 8A and B, respectively. It could be seen that with an increment of electric signal frequency, the WGM resonance dips shift toward longer wavelength region.

From Figure 8A, it is obvious that as electric signal frequency ranges from 2 kHz to 14 kHz, WGM resonance dips show more obvious regular shift at higher applied electric field strength. And the maximum WGM resonance wavelength shift reaches 1.1845 nm at 4.1 V μm^{-1}. When electric signal frequency is larger than 14 kHz, WGM resonance dips show similar frequency-dependent wavelength shift behaviors at different applied electric field strengths. When electric signal frequency increases from 14 kHz to 30 kHz, the WGM resonance wavelength shift reaches 0.7545 nm, while as electric signal frequency ranges from 30 kHz to 40 kHz, the WGM resonance dips show no obvious wavelength shift with only irregular fluctuations.

From Figure 8B, it could be seen that WGMs in the microresonators filled with DFLC-2 are no longer supported at 1 V μm^{-1} when electric signal frequency is less than 10 kHz. As electric signal frequency ranges from 10 kHz to 50 kHz, WGM resonance dips show similar wavelength shift behaviors at different applied electric field strengths. When electric frequency ranges from 10 kHz to 32 kHz, WGM resonance dips shift regularly with the increment of electric signal frequency. The WGM dips move toward longer wavelength region by 2.396 nm at an applied electric field strength of 4 V μm^{-1}. As applied electric signal frequency ranges from 32 kHz to 50 kHz, WGM resonance wavelengths exhibit no obvious shift with only irregular fluctuations.

5 Conclusions

We have proposed that for MOF-based microresonators, the crossover frequency and Freedericksz transition
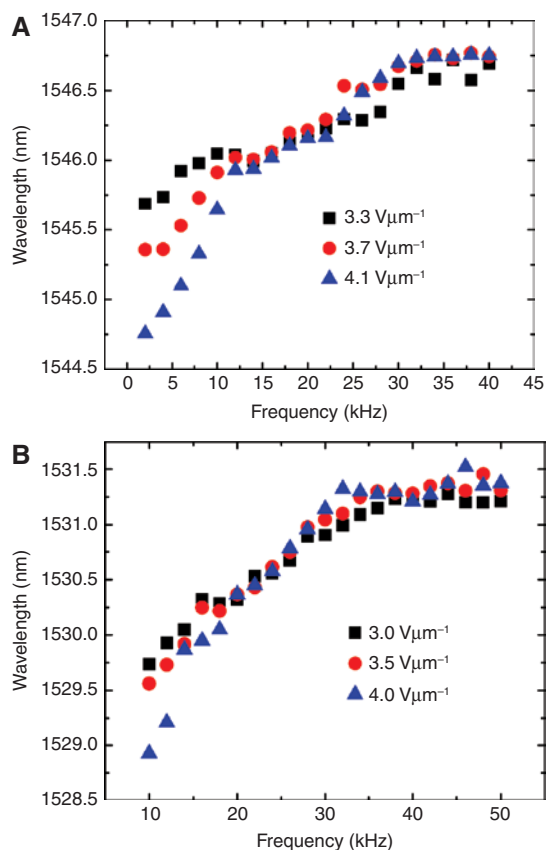
Figure 8: WGM resonance wavelength as functions of applied electric field frequency under different electric field intensities for grapefruit-MOF-based microresonators filled with (A) DFLC-1 and (B) DFLC-2, respectively.

threshold properties of DFLCs should be investigated. The crossover frequency of DFLC-1 is about 20 kHz, and the crossover frequency of DFLC-2 is between 20 kHz and 30 kHz. The Freedericksz transition thresholds of DFLC-1 and DFLC-2 are 1.8 V μm^{-1} and 1.0 V μm^{-1}, respectively. When the applied electric signal frequency is below the crossover frequency, WGM resonance dips show wavelength shift toward shorter wavelength region as the applied electric field is strengthened. However, when applied electric field frequency is larger than the crossover frequency, WGM resonance dips start to move toward longer wavelength with the increment of the applied electric field intensity. This property could be exploited for the design of bi-directional wavelength-tunable devices. In addition, the proposed electrically tunable micro-cavity integrated with DFLCs is anticipated to find potential applications in optical filtering, all-optical switching, as well as electrically controlled micro-optics devices.

References

[1] Spillane SM, Kippenberg T J, Vahala KJ. Ultralow-threshold Raman laser using a spherical dielectric microcavity. Nature 2002;415:621–3.

[2] Pöllinger M, O'Shea D, Warken F, Rauschenbeutel A. Ultrahigh-Q tunable whispering-gallery-mode microresonator. Phys Rev Lett 2009;103:1.

[3] Liu Y, Davanço M, Aksyuk V, Srinivasan K. Electromagnetically induced transparency and wideband wavelength conversion in silicon nitride microdisk optomechanical resonators. Phys Rev Lett 2013;110:223603.

[4] Cai DP, Lu JH, Chen CC, Lee CC, Lin CE, Yen TJ. High Q-factor microring resonator wrapped by the curved waveguide. Sci Rep 2014;5:10078.

[5] Shopova SI, White IM, Sun Y, et al. On-column micro gas chromatography detection with capillary-based optical ring resonators. Anal Chem 2008;80:2232–8.

[6] Savchenkov AA, Ilchenko VS, Handley T, Maleki L. Second-order filter response with series-coupled silica microresonators. IEEE Photonics Technol Lett 2003;15:543–4.

[7] Hryniewicz JV, Absil PP, Little BE, Wilson RA, Ho PT. Higher order filter response in coupled microring resonators. IEEE Photonics Technol Lett 2000;12:320–2.

[8] Chen R, Van Duong T, Sun HD. Single mode lasing from hybrid hemispherical microresonators. Sci Rep 2012;2:244.

[9] Li M, Wu X, Liu L, Fan X, Xu L. Self-referencing optofluidic ring resonator sensor for highly sensitive biomolecular detection. Anal Chem 2013;85:9328–32.

[10] Fan X, White IM, Shopova SI, Zhu H, Suter JD, Sun Y. Sensitive optical biosensors for unlabeled targets: a review. Anal Chim Acta 2008;620:8–26.

[11] Jia Y, Hanka K, Zawilski KT, Schunemann PG, Buse K, Breunig I. Continuous-wave whispering-gallery optical parametric oscillator based on CdSiP2. Opt Express 2018;26:10833–41.

[12] White IM, Gohring J, Sun Y, Yang G, Lacey S, Fan X. Versatile waveguide-coupled optofluidic devices based on liquid core optical ring resonators. Appl Phys Lett 2007;91:2411041–3.

[13] Kiraz A, Kurt A, Dündar MA, Demirel AL. Simple largely tunable optical microcavity. Appl Phys Lett 2006;89:081118.

[14] Pinnick RG, Biswas A, Chýlek P, et al. Stimulated Raman scattering in micrometer-sized droplets: time-resolved measurements. Opt Lett 1988;13:494–6.

[15] Hopkins RJ, Symes R, Sayer RM, Reid JP. Determination of the size and composition of multicomponent ethanol/water droplets by cavity-enhanced Raman scattering. Chem Phys Lett 2003;380:665–72.

[16] Liu Y, Shi L, Xu X, et al. All-optical tuning of a magnetic-fluid-filled optofluidic ring resonator. Lab Chip 2014;14:3004–10.

[17] Lin W, Zhang H, Liu B, et al. Laser-tuned whispering gallery modes in a solid-core microstructured optical fibre integrated with magnetic fluids. Sci Rep 2015;5:17791.

[18] Mahmood A, Kavungal V, Ahmed SS, Farrell G, Semenova Y. Magnetic-field sensor based on whispering-gallery modes in a photonic crystal fiber infiltrated with magnetic fluid. Opt Lett 2015;40:4983–6.

[19] Humar M, Ravnik M, Pajk S, Muševič I. Electrically tunable liquid crystal optical microresonators. Nat Photonics 2009;3:595–600.

[20] Kumar TA, Mohiddon MA, Dutta N, Viswanathan NK, Dhara S. Detection of phase transitions from the study of whispering gallery mode resonance in liquid crystal droplets. Appl Phys Lett 2015;106:051101.

[21] Yang C, Zhang H, Liu B, lin S, Li Y, Liu H. Electrically tunable whispering gallery mode microresonator based on a grapefruit-microstructured optical fiber infiltrated with nematic liquid crystals. Opt Lett 2017;42:2988–91.

[22] Meyer RB. On the existence of even indexed disclinations in nematic liquid crystals. Philos Mag 1973;27:405–24.

[23] Williams C, Pierański P, Cladis PE. Nonsingular S=+1 Screw disclination lines in nematics. Phys Rev Lett 1972;29:90–2.

[24] Allender DW, Crawford GP, Doane JW. Determination of the liquid-crystal surface elastic constant K24. Phys Rev Lett 1991;67:1442–5.

[25] Crawford GP, Allender DW, Doane JW. Surface elastic and molecular-anchoring properties of nematic liquid crystals confined to cylindrical cavities. Phys Rev A 1992;45:8693–708.

[26] Cladis PE, Kléman M. Non-singular disclinations of strength S=+1 in nematics. J Phys (Paris) 1972;33:591–8.

[27] Lam CC, Leung PT, Young K. Explicit asymptotic formulas for the positions, widths, and strengths of resonances in Mie scattering. J Opt Soc Am B 1992;9:1585–92.

[28] Zhang YX, Pu XY, Feng L, Han DY, Ren YT. Polarization characteristics of whispering-gallery-mode fiber lasers based on evanescent-wave-coupled gain. Opt Express 2013;21:12617–28.

[29] Mahmood A, Kavungal V, Ahmed SS, et al. Magnetic field sensing using whispering-gallery modes in a cylindrical microresonator infiltrated with ferronematic liquid crystal. Opt Express 2017;25:12195–202.

[30] Bücher HK. Frequency-addressed liquid crystal field effect. Appl Phys Lett 1974;25:186.

[31] Schadt M. Dielectric heating and relaxations in nematic liquid crystals. Mol Crystals Liquid Crystals 1981;66:319–36.

[32] Zolina V. Forces causing the orientation of an anisotropic liquid. Trans Faraday Soc 1933;29:919–30.